Spin dynamics in the alternating chain system $Li_3Cu_2SbO_6$ with defects probed by nuclear magnetic resonance

E. Vavilova,[1] S. Nishimoto,[2,3] T. Salikhov,[1] T. Vasilchikova,[4] V. Nalbandyan,[5] A. Vasiliev,[4,6] and E. Zvereva[4,*]

[1]*Zavoisky Physical-Technical Institute, FRC Kazan Scientific Center of RAS, 420029 Kazan, Russia*

[2]*Department of Physics, Technical University Dresden, 01069 Dresden, Germany*

[3]*Institute for Theoretical Solid State Physics, IFW Dresden, 01069 Dresden, Germany*

[4]*Faculty of Physics, Moscow State University, Moscow 119991, Russia*

[5]*Faculty of Chemistry, Southern Federal University, Rostov-on-Don 344090, Russia*

[6]*National Research South Ural State University, Chelyabinsk 454080, Russia*

(Received 9 November 2020; revised 15 February 2021; accepted 22 February 2021; published 10 March 2021)

We report the results of the detailed measurements of ^{7}Li nuclear magnetic resonance (NMR) spectra, NMR line shift, spin-lattice relaxation rate, bulk magnetization, magnetic susceptibility, and heat capacity on the spin-$\frac{1}{2}$ Heisenberg honeycomb compound $Li_3Cu_2SbO_6$. This system consists of weakly coupled alternating Cu chains and, owing to the site inversion, some of the magnetic Cu ions are substituted by nonmagnetic Li ions. As a result, the effective spin model for $Li_3Cu_2SbO_6$ is a set of Cu alternating chain fragments of different length (the "chain-segments spin model"). Due to this unique structure, various kinds of peculiar magnetic features arise and the combination of local (NMR) and global experimental techniques is especially effective in their study. In order to describe the experimental results theoretically, we perform full diagonalization calculations for the chain-segments spin model taking explicit account of all of the possible dimerized chain fragments of different length. From the fitting of measured susceptibility, we estimate the exchange interactions as $J_{FM} = -244$ K and $J_{AF} = 146$ K, and find that about 19% of magnetic Cu ions are replaced by nonmagnetic Li ions. Using those values, we can even quantitatively reproduce the observed NMR line shift and the specific heat as well as field- and temperature-dependent magnetization over a wide temperature range. Although small deviations are seen at very low temperature, they can be corrected by considering the effect of small interchain interactions.

DOI: 10.1103/PhysRevB.103.094415

I. INTRODUCTION

Two-dimensional (2D) compounds as the widest class of low-dimensional magnets demonstrate a huge variety of the geometry of magnetic subsystems. Some of these lattices create a geometrical competition of different exchange interactions, which leads to so-called magnetic frustration phenomena and possible exotic ground states. A striking example of a frustrated lattice is a honeycomb geometry of magnetic ions in layers. A honeycomb lattice occupies a special place among quasi-2D materials because quantum fluctuations in it are enhanced due to the particular coordination number ($z = 3$). Such a lattice contains a triangular motif, but in the case of a symmetric cell with antiferromagnetic (AF) nearest-neighbor interactions there is no frustration and the ground state is the Néel antiferromagnet. At the same time, if one takes into account the next-nearest-neighbor interaction, as well as the difference in the nearest-neighbor interactions in different faces of the hexagon, topological frustration arises in the honeycomb lattice and, as a consequence, a wide variety of types of magnetic structures can be realized [1–6].

In particular, several honeycomb systems like $Na_2Cu_2TeO_6$ [7] and $Na_3Cu_2SbO_6$ [8,9] have been recently discovered, where a quasi-one-dimensional structure arises as a result of the interplay of lattice distortion, an orbital arrangement, and frustration. In these compounds, two dominant couplings of Cu^{2+} ions occur along the Cu-O-Sb(Te)-O-Cu-O-Cu superexchange path [10]. In such configuration one can expect an AF-AF or AF-ferromagnetic (FM) alternating chain model depending on the sign and ratio of the largest exchange integrals. An alternative model involves weakly interacting dimers, when one of the exchange integrals is much larger than the other. In the case of an AF-FM alternating chain with the FM largest exchange interaction, it has been theoretically suggested that the Haldane conjecture is well applicable to the system [11,12]. All of these models are characterized by the presence of a spin gap in the spectrum of magnetic excitations. Due to the presence of an energy gap, the magnetic susceptibility of the system vanishes at low temperature.

Based on experimental studies of magnetic susceptibility [7,9], heat capacity [9], and inelastic neutron scattering [13], the applicability of the alternating chain model for $Na_2Cu_2TeO_6$ and $Na_3Cu_2SbO_6$ has been proved. As for the sign of exchange integrals, both the AF-AF and AF-FM models are considered as a good description of the system in previous experimental and computational studies [10,13,14]. However, the AF-FM model with larger FM exchange

*Deceased.

interaction may be most likely from the viewpoint of experiments. Nuclear magnetic resonance (NMR) as a local method proved to be an effective component of complex studies of spin-gap systems, for example, Haldane chains [15–17], dimer chains [18,19], and alternating spin-$\frac{1}{2}$ chains [20,21]. Indeed, NMR studies of $Na_2Cu_2TeO_6$ [22] and $Na_3Cu_2SbO_6$ [23] compounds gave clear evidence of a spin-gapped behavior of local static and dynamic susceptibility of the Cu subsystem in the frame of the AF-FM alternating chain scenario.

Another fascinating honeycomb system is $Li_3Cu_2SbO_6$, which was first synthesized in the late 1990s [24]. This paper presents a detailed experimental and theoretical study of the magnetic properties of this compound. $Li_3Cu_2SbO_6$ is isotypic with $Na_3Cu_2SbO_6$ [8] and crystallizes in the space group $C2/m$ [25,26]. However, as it often happens in structures containing lithium and copper ions, the Li and Cu atoms are partially mixed in $Li_3Cu_2SbO_6$. Since the Li ion acts as a nonmagnetic defect, the lithium substitution results in a segmentation of the Cu chains into fragments of different length and gives rise to uncompensated spins at the segment ends similar to the well-known nonmagnetic substitution effect in planar cuprates [27–29] and nickel chains [30–33]. Due to the sufficiently large correlation length in spin chains, these spins cannot just be point defects, but lead to the formation of more complex magnetic objects consisting of neighboring spins (trimers and longer clusters) that separate spin-gapped regions of the chain [34]. Thus, defects in spin chains can lead to a number of nontrivial phenomena, from phase separation into gapped and superparamagnetic segments [17,35] to the formation of impurity induced antiferromagnetic order [36–38].

Since huge Curie-like contribution of unpaired Cu moments and clusters masks the component from the gapped spin matrix in bulk magnetic susceptibility in the $Li_3Cu_2SbO_6$ compound, it is difficult to use this technique for determination of the detailed magnetic structure [9,24]. Using the combination of global (DC susceptibility) and local magnetometry methods and precise control and analysis of the structure [x-ray diffraction (XRD)] Koo *et al.* [26] detected the presence of a spin-gapped contribution to magnetic behavior. The alternating spin chain scenario for description of $Li_3Cu_2SbO_6$ was tested using the obtained data. However, since both experimental methods of studying of global and local magnetization detect the response of copper spins, the researchers also faced the problem of the vanishingly small contribution of the gapped matrix at low temperatures. Instead, the application of NMR for studying the magnetism of $Li_3Cu_2SbO_6$ would be more informative in this situation because it can obtain a distant view of the magnetic system by recording a signal from the nuclei of a nonmagnetic lithium ion. Using various experimental protocols, it is possible to register the contributions of different components of the magnetic subsystem separately by examining both the static component of the local susceptibility and the low-frequency part of the spin excitation spectrum. In fact, NMR has been successfully applied for studying the effect of different kinds of defects in spin chains [32,39–42], including the isostructural compound $Na_2Cu_2TeO_6$ [22].

The magnetic properties of simple Heisenberg chain segments have been intensively investigated by theory [40,43–48]. However, completely different ground-state and thermodynamic properties would be expected for AF-AF or AF-FM dimerized chain segments. Therefore, a new spin model needs to be built for the fragmented chain compound $Li_3Cu_2SbO_6$.

In this paper we study the magnetic properties of the $Li_3Cu_2SbO_6$ compound by measuring bulk magnetization, magnetic susceptibility, heat capacity under magnetic fields, as well as local static and dynamic susceptibility registered by ^{7}Li NMR. In order to describe the experimental measurements quantitatively, we introduce a spin model consisting of gapped and nongapped dimerized chain segments, where the Li and Cu ions are regarded as nonmagnetic and magnetic sites, respectively. From the fitting of measurements, we estimate the exchange interactions of a dimerized chain as $J_{\mathrm{FM}} = -244$ K and $J_{\mathrm{AF}} = 146$ K, and also find that about 19% of magnetic Cu ions are replaced by nonmagnetic Li ions. Furthermore, we discuss a possible effect of small interchain interactions.

The paper is organized as follows. Experimental details are summarized in Sec. II. Results of ^{7}Li NMR, thermodynamic, and magnetometry experiments are presented in Sec. III. In Sec. IV, a microscopic spin model is given and full exact diagonalization calculations for the spin model are performed. The consistency of calculated results and experimental measurements is also discussed. The conclusions are summarized in Sec. V.

II. EXPERIMENTAL DETAILS

A polycrystalline $Li_3Cu_2SbO_6$ sample was synthesized using a solid-state reaction technique and its crystal structure (Fig. 1) was characterized by powder XRD using the Rietveld method, as reported previously [26]. A partial Cu/Li site inversion was found in the sample: 17% of copper structural positions are occupied by lithium ions.

NMR experiments on the $Li_3Cu_2SbO_6$ powder sample were performed using the Tecmag Redstone solid-state pulse spectrometer and a resistive magnet (0–2 T) from Bruker at fixed fields $B = 0.725$ and 1.45 T. The homemade helium flow cryostat with automatic temperature stabilization in the range 3–320 K was used for temperature control. The NMR spin-echo signal was obtained on ^{7}Li nuclei and has a nuclear spin $I = 3/2$ (natural abundance 92.58%) and a quadruple moment $Q = -0.04$ b [49]. The spectra were recorded by Fourier transformation of the solid echo at high temperatures and by integrating the spin-echo intensity at each point of the step-by-step frequency sweeping at low temperatures where the NMR linewidth exceeds the width of the circuit characteristic. The longitudinal relaxation time T_1 was measured on the maximum of spectral intensity by inversion recovery and simulated echo techniques.

The magnetic measurements were performed by means of a superconducting quantum interference device magnetometer (MPMS XL-5, Quantum Design). The temperature dependencies of magnetic susceptibility were measured at the magnetic fields $B = 0.1$, 0.725, 1.45, 3, 5, and 7 T in the temperature range 2–70 K. The isothermal magnetization was obtained for magnetic fields $B \leqslant 9$ T at $T = 2$ K after cooling the sample in zero field with a Quantum Design PPMS 9 system.

Specific-heat measurements were carried out by a relaxation method using a Quantum Design PPMS 9. The data

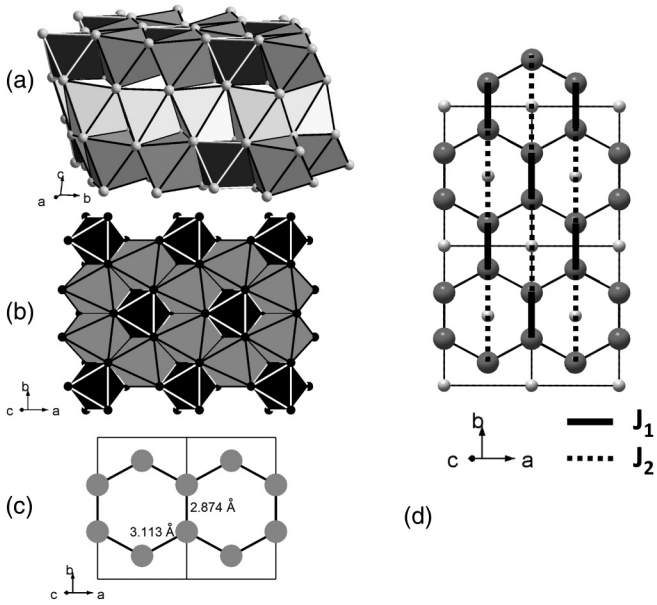

FIG. 1. Crystal structure [26] of $Li_3Cu_2SbO_6$. (a) Polyhedral presentation: Black octahedra are SbO_6; gray octahedra are CuO_6 with Li partially substituting for Cu; white octahedra are LiO_6 with Cu partially substituting for Li; white balls are oxygen atoms. (b) The honeycomb layer Cu_2SbO_6 with about 17% Li substituting for Cu. (c) The honeycomb layer with Cu/Li positions only. (d) The honeycomb layer with the directions of the strongest exchange interactions; here big dark gray circles are Cu ions and small light gray circles are Sb ions.

were collected at zero magnetic field in the temperature range 2–280 K.

III. EXPERIMENTAL RESULTS AND DISCUSSION

A. Static magnetization and specific heat

Temperature dependencies of static susceptibility of $Li_3Cu_2SbO_6$ at different external magnetic fields are presented in Fig. 2.

The measured magnetization isotherm $M(B)$ at $T = 2$ K for $Li_3Cu_2SbO_6$ is presented in Fig. 3. It has a slightly S-shaped form and shows neither hysteresis nor saturation in the magnetic fields up to 9 T. Within this range of the applied magnetic field, the magnetic moment is still far below the theoretically expected saturation magnetic moment for Cu^{2+} ($S = 1/2$): $M_{\rm sat} = ngS\mu_B = 2.2\mu_B$ (where $n = 2$ is the number of magnetic centers for $Li_3Cu_2SbO_6$ and g and μ_B are the effective g factor and Bohr magneton, respectively). This is due to the fact that spin-singlet pairs of antiferromagnetically coupled Cu^{2+} ions survive at $B < 9$ T. More details are explained in Sec. IV F.

The temperature dependence of the specific heat $C_p(T)$ at zero magnetic field for $Li_3Cu_2SbO_6$ is shown in Fig. 4. In agreement with previously reported magnetic susceptibility data [26] there are no anomalies corresponding to phase transitions. Over the whole temperature range studied, the $C_p(T)$ curve grows monotonously. It is worth noting that the specific heat at 280 K is still considerably lower than a classical Dulong-Petit saturation value $C = 3R\nu = 224\,{\rm J/(mol\,K)}$, where $R = 8.31\,{\rm J/(mol\,K)}$ is the gas constant and $\nu = 12$ is the number of atoms per formula unit in $Li_3Cu_2SbO_6$.

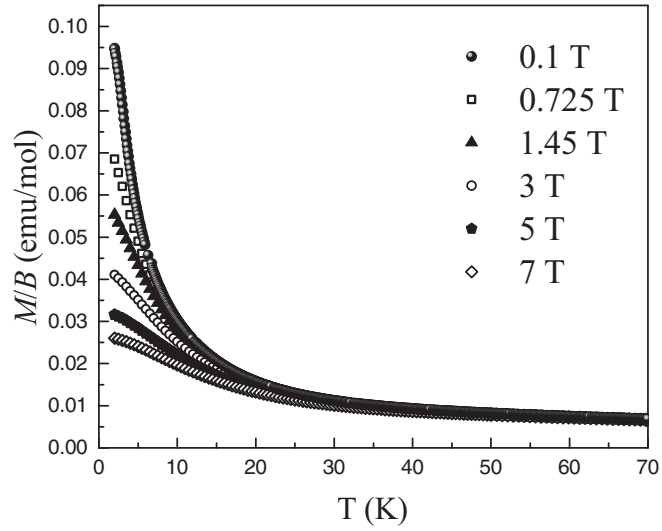

FIG. 2. Temperature dependencies of static susceptibility of $Li_3Cu_2SbO_6$ at external magnetic field $B = 0.1$, 0.725, 1.45, 3, 5, and 7 T.

We assume that the total specific heat consists of two different contributions $C_p = C_{\rm lat} + C_{\rm mag}$, where lattice contribution $C_{\rm lat}$ due to acoustic and optical phonons and a magnetic contribution $C_{\rm mag}$ can be related to the AF-FM alternating $S = 1/2$ Cu^{2+} spin chains. It was found that the best description of the lattice contribution $C_{\rm lat}$ (solid line in Fig. 4) is achieved by the sum of the Debye (C_D) and Einstein (C_E) contributions [50]:

$$C_{\rm lat} = \alpha C_D(T, \Theta_D) + (1-\alpha)\sum_i C_{Ei}(T, \Theta_{Ei}), \qquad (1)$$

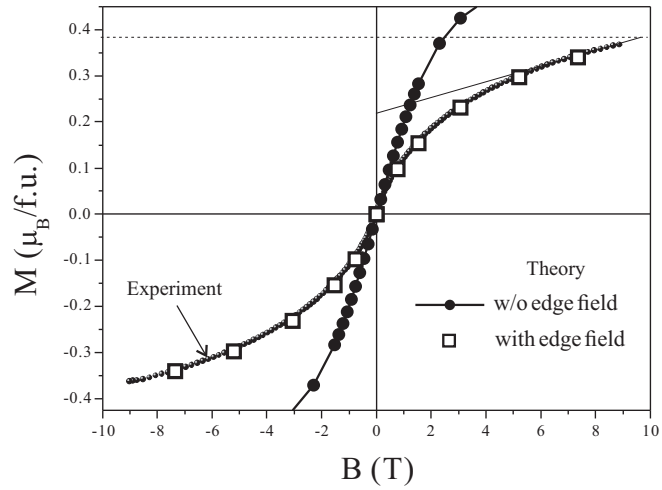

FIG. 3. Magnetization isotherm at $T = 2$ K for $Li_3Cu_2SbO_6$ (small black filled symbols). The filled circles and open squares correspond to calculations within the framework of the chain-segments spin model (see Sec. IV F).

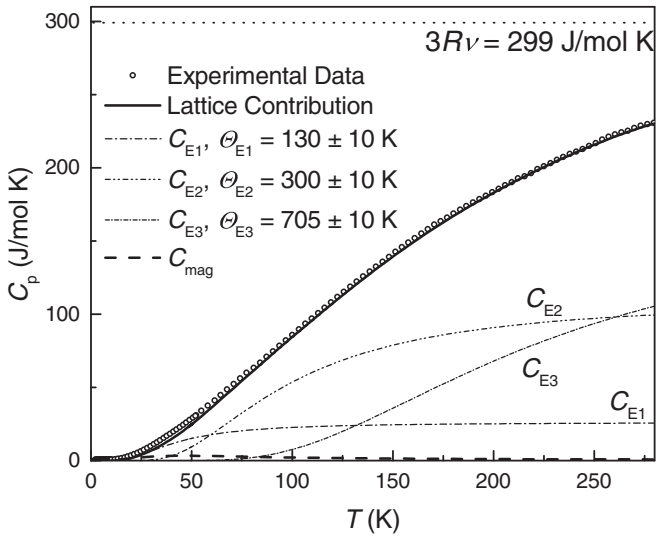

FIG. 4. The temperature dependence of the specific heat $C_p(T)$ (open circles) at zero magnetic field in $Li_3Cu_2SbO_6$. The solid line represents the lattice contribution C_{lat} described by the sum of Debye (not shown) and three Einstein functions C_{E1}, C_{E2}, and C_{E3}. The dashed line corresponds to magnetic contribution C_{mag}.

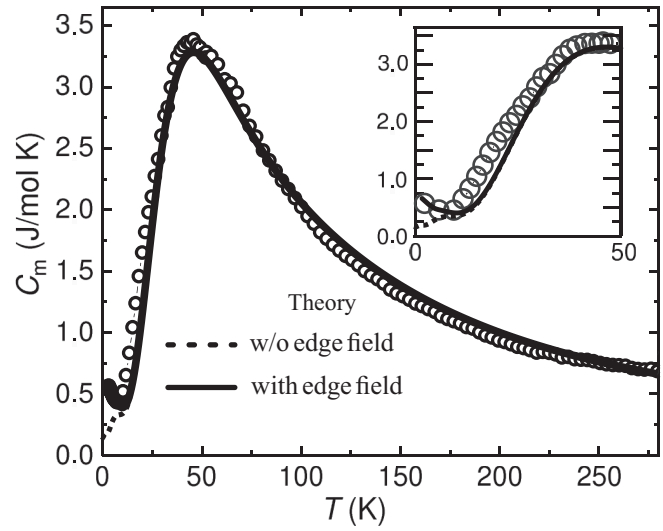

FIG. 5. The temperature dependence of magnetic specific heat $C_{mag}(T)$ (black open symbols). Solid and dashed lines represent the results of calculations within the framework of the chain-segments spin model (see Sec. IV E). Inset: Enlarged view at low temperature.

where Θ_D and Θ_{Ei} are the Debye and Einstein temperatures, respectively, and α is a relative weight factor for the Debye and Einstein terms.

Our best fit of experimental data according to Eq. (1) reveals the Debye temperature $\Theta_D = 580 \pm 10$ K, which is in reasonable agreement with values for other Li-based honeycomb compounds $Li_3Ni_2SbO_6$ [51] and $Li_3Co_2SbO_6$ [52]. The three Einstein terms are characterized by temperatures $\Theta_{E1} = 130 \pm 10$ K, $\Theta_{E2} = 300 \pm 10K$, and $\Theta_{E3} = 705 \pm 10$ K and presented by different dash-dotted lines in Fig. 4. The Debye component is not shown due to its relatively small value in comparison with Einstein terms in the wide temperature range.

The magnetic part of the specific heat C_{mag} for $Li_3Cu_2SbO_6$ was obtained by subtracting the C_{lat} from the total $C_p(T)$ (Fig. 5). The pronounced peak in the magnetic specific-heat curve at $T \sim 45$ K can be ascribed to short-range correlations in the studied system. More details are discussed in Sec. IV E.

B. Nuclear magnetic resonance

The crystal structure of $Li_3Cu_2SbO_6$ contains two positions of Li in between the Cu-Sb planes with a slightly different copper and oxygen environment. In a powder sample, the positions of the signals from these two lithium nuclei are not resolved and are located inside one inhomogeneously broadened line, the width of which at room temperature is about 10 kHz. The quadrupole splitting is less than 25 kHz and the satellites are inside the total linewidth. The spectrum shape remains Gaussian-like down to the lowest temperatures and does not contain the broad wings that are often observed in the NMR spectra of chains with a small number of defects [53]. The lithium nuclei in the copper position (defects) do not seem to make a notable contribution to the spectrum intensity because of their fast spin-lattice relaxation due to the close proximity of magnetic copper ions.

The line shift K is created by the static part of the averaged local field on Li position and can be defined as $K = (\omega - \omega_L) \times 100/\omega_L$ (%) where ω_L is a Larmor frequency and ω is the position of the maximum of the line intensity. The line shift can be written as a function of the spin susceptibility of the magnetic ions, which produce the internal field in a nuclei position:

$$K(T) = K_0 + \frac{A_{hf}}{N_A}\chi_{spin}(T), \tag{2}$$

where K_0 is the temperature-independent part that is related to the Van Vleck susceptibility and the second-order quadrupolar effects, A_{hf} is the on-site ^{7}Li hyperfine coupling, and N_A is the Avogadro constant. The measured NMR spectra at $B = 0.725$ T and linewidth at $B = 0.725$ and 1.45 T are shown in Fig. 6. In both magnetic fields, the spectrum intensity maximum shifts to higher frequency and the lines broaden with decreasing temperature. At the temperature of about 75 K at 0.725 T and 45 K at 1.45 T, the line shift has a wide maximum and turns towards reducing with further cooling [Figs. 7(a) and 8]. Finally, at $T < 15$ K the line shift becomes negative.

Bulk magnetic susceptibility dependence of the NMR line shift reflects a stepwise transformation in the regimes of the magnetic subsystem with a temperature. As shown in the previous work [26], bulk static magnetic susceptibility contains contributions from two magnetic subsystems: spin-gapped fragments of the magnetic chains χ_{chain} and quasifree spins associated with chain breaks (or short nongapped segments) χ_{CW} noticeable at low temperatures. Interlayer lithium can be located close to the gapped chain segments or close to defects. Due to the small distance from the second kinds of lithium positions to quasifree copper spins at the chain breaks, the hyperfine field on them is sufficiently large and one can expect

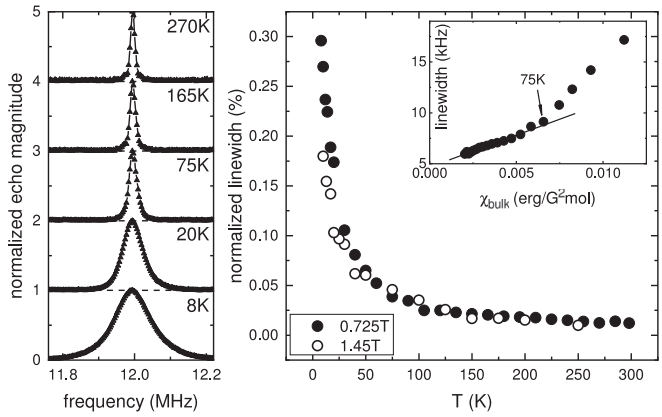

FIG. 6. Temperature transformation of ^{7}Li powder NMR spectra measured at the external field of 0.725 T (left panel). Temperature dependence of the linewidth normalized to the measurement frequency at the external fields of 0.725 T and 1.45 T (right panel). Inset: Linewidth at 0.725 T vs bulk static susceptibility [26].

fast longitudinal and transverse relaxation of lithium nuclear spins at these positions.

Therefore, their contribution to spin-echo detected spectra is low and we can attribute the obtained data mostly to lithium nuclei which are close to the relatively long chain segments. This assumption is supported by the fact that at temperature range 50–270 K the line shift matches well enough the susceptibility of alternating chains χ_{chain} [26] [Fig. 7(b)]. At low temperatures the sign of the slope of χ dependence of the line shift changes and the shift value becomes negative, indicating a drastic change in the geometry of the magnetic subsystem. Indeed, since most of the gapped chain segments become mainly nonmagnetic at low temperatures, the average local field on lithium nuclei is no longer determined by interaction with nearest-neighbor copper ions, but with quasifree spins of defects and short nongapped segments (trimers, etc.). In this case, the length and angle characterizing the hyperfine

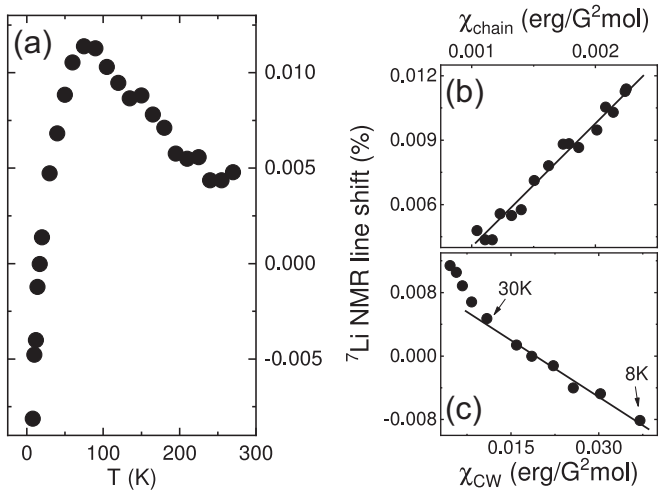

FIG. 7. Temperature dependence of the NMR line shift at 0.725 T (left panel) and DC bulk magnetic susceptibility measured at the same field (right panel). Solid lines indicate the regions of linearity.

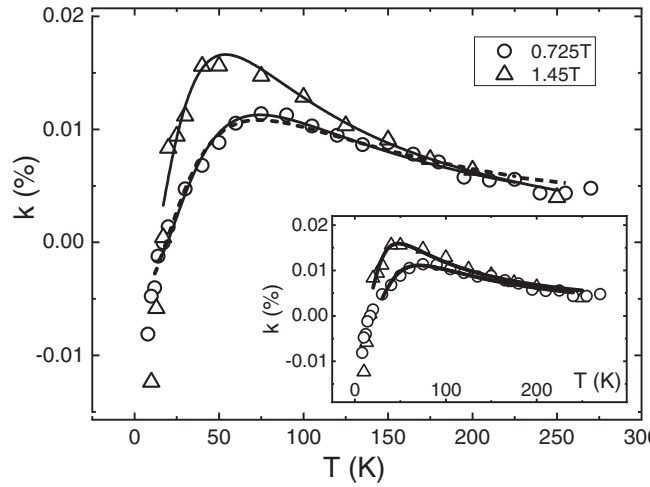

FIG. 8. Temperature dependence of the NMR line shift at 0.725 and 1.45 T. Solid lines represent the fits to Eq. (4); the dashed line is a fit to Eq. (3). Inset: Solid lines represent the fits by the dimer model (see text).

interaction change dramatically, which causes a transformation of the magnitude and direction of the local-field values on the lithium nuclei or, in other words, transformation of the hyperfine tensor. Below 30 K the line shift is proportional to Curie-Weiss contribution to bulk susceptibility χ_{CW} taken from [26] [Fig. 7(c)]. The values of the negative shift normalized to the external fields 0.725 and 1.45 T (not shown) coincide within the experimental error. It confirms the origin of the signal from free spins below 20 K.

Assuming that NMR as a local selective method allows one to study the susceptibility of alternating chains more accurately and in a wider temperature range than the bulk technique, one can follow the the procedure proposed in the work [23] for the isostructural compound $Na_3Cu_2SbO_6$. To approximate the temperature dependence of the line shift $K_{\text{spin}}(T)$, which is proportional to the local static susceptibility, three models of alternating chains were tested (Fig. 8): with two antiferromagnetic exchange interactions of different magnitudes (AF-AF); with alternating antiferromagnetic and ferromagnetic interactions (AF-FM); and, as a limiting case, the alternating dimer model. According to the previous work by Hall *et al.* [54], the static spin susceptibility and thereby NMR line shift for AF-AF chain obeys the formula

$$K_{\text{spin}}(T) = \frac{1}{T}\frac{A + Bx + Cx^2}{1 + Dx + Ex^2 + Fx^3} \tag{3}$$

where $x = |J_1|/T$, J_1, and J_2 are interchain exchange integrals and A and F are numeric parameters dependent on $\alpha_{\text{AF-AF}} = J_2/J_1$. Fitting the temperature dependence of the line shift at 0.725 T one can obtain $J_1 = 57.9$ K, $J_2 = 25.5$ K, and gap value $\Delta_{\text{AF-AF}} = J_1(1 - \frac{1}{2}\alpha_{\text{AF-AF}} - \frac{5}{16}\alpha^2_{\text{AF-AF}}) = 48.7$ K.

Similarly, for AF-FM chains we adopt the formula [55]

$$K_{\text{spin}}(T) = \frac{A'y^3 + B'y^2 + C'y + D'}{y^4 + E'y^3 + F'y^2 + G'y + H'}, \tag{4}$$

where $y = T/|J_{\text{FM}}|$ and A' and H' are numeric parameters dependent on $\alpha_{\text{AF-FM}} = J_{\text{FM}}/J_{\text{AF}}$. Fitting the temperature dependence of the line shift at 0.725 T one can obtain

$J_{FM} = -159$ K, $J_{AF} = 130$ K, and gap value $\Delta_{FM-AF} = |J_{FM}|(1 - \frac{1}{2}\alpha_{AF-FM} + \frac{3}{16}\alpha^2_{AF-FM}) = 87$ K.

Approximation within the framework of the noninteracting spin dimer model [23] $K_{spin} \propto 1/T[3 + \exp(\Delta_{dimer}/T)]$ gives $\Delta_{dimer} = 113.45$ K for 0.725 T and 76.74 K for 1.45 T.

All three models give an acceptable description of the temperature dependence of the line shift, but the values of the energy gap and exchange integrals obtained for the AF-AF model are small. The dimer model is in good agreement with the experiment at $T > 45$ K but strongly deviates from the experimental points below this temperature. In contrast, parameters obtained for the AF-FM model in temperature range 35–270 K are in better agreement with the values of exchange integrals obtained by fitting the bulk static susceptibility of chains [26]: $\chi_{chain} = \chi - \chi_{CW}$ where $J_{FM} = -285$ K, $J_{AF} = 160$ K. That makes it possible to choose the AF-FM model as the best description of the alternating chains. The values obtained from the NMR line shift seem to be more correct than ones from the bulk susceptibility, since they are less affected by the contribution of paramagnetic segments and defects.

The maximum in the temperature dependence of the line shift measured at 1.45 T moves towards the lower temperatures (≈50 K) compared to the data obtained at 0.725 T. This strong field dependence, strictly speaking, does not allow directly applying Eq. (4); however, using it formally one can get the following values of exchange integrals: $J_{FM} = -157$ K, $J_{AF} = 99$ K. Such a strong decrease in the antiferromagnetic interaction parameter demonstrates the effective suppression of antiferromagnetic coupling in the AF-FM chains by external magnetic field. The magnitude of the external field in energy units is significantly smaller than the gap obtained from Eq. (4) describing an infinite AF-FM chain. Therefore, the unexpectedly strong field dependence demonstrates the importance of taking into account the fragmentation of the chain by nonmagnetic defects when simulating the physical properties of the system.

In contrast to the line shift, the temperature dependence of the ^{7}Li NMR linewidth $\Delta\omega(T)$ for both magnetic fields does not show any maximum but increases steadily with lowering temperature (right panel of Fig. 6). The coincidence of two presented curves indicates the paramagnetic nature of the inhomogeneous line broadening. The linewidth being originated by the distribution of the local fields is much more sensitive to the presence of quasifree spins of chain defects as well as the magnetic moments of short nongapped chain segments than the shift of the line maximum created by averaged local field. Indeed, the linewidth follows the experimentally determined bulk susceptibility at high temperature down to 90 K and grows slightly faster than a Curie-Weiss law below this temperature. This additional rise in the linewidth suggests that the magnetic subsystem gradually incorporates the large magnetic moments of short nongapped chain fragments such as triplets.

The dynamics of the spin system was studied by examining ^{7}Li nuclear spin-lattice relaxation. The longitudinal relaxation rate T_1^{-1} was measured at the maximum of the spectral intensity in the external magnetic field 1.45 T. The inhomogeneously broadened spectrum contains not only the main transition but unresolved quadrupole satellites. Therefore it is impossible to measure the relaxation rate separately on the central line of the spectrum. For this reason, in the fitting procedure we used a stretched exponential function $M(t) = M_0 \exp(-t/T_1)^\beta$, where T_1 is an effective spin-relaxation time and β is a parameter related to the distribution of magnetic relaxation rates due to overlapping of the spectrum components and to the spatial distribution of the magnetic centers creating the local field. Relaxation slows down below 200 K with a minimal rate registered around 15 K (Fig. 9). With further lowering temperature, a sharp upturn of the relaxation is observed.

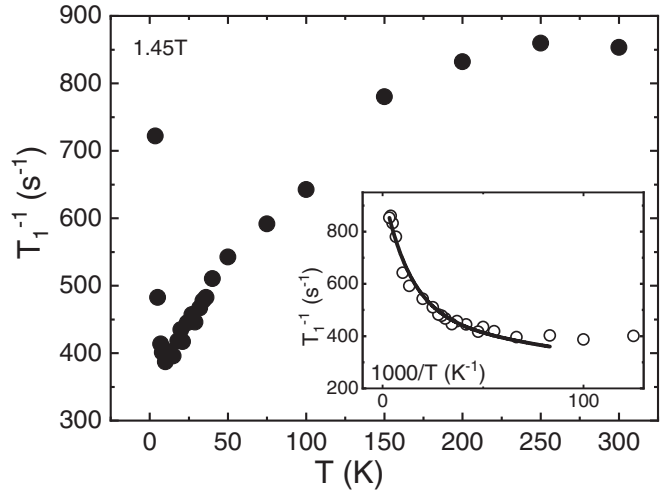

FIG. 9. ^{7}Li nuclear spin-lattice relaxation as a function of temperature. Inset: Relaxation rate vs inverse temperature. The solid line represents a fit to Eq. (5).

The temperature dependence of the nuclear relaxation rate T_1^{-1} at 1.45 T can be fitted by a combination of the activation law describing the gapped behavior of chain segments and Curie-Weiss contribution of nongapped chain segments and paramagnetic centers at the segment ends:

$$T_1^{-1} = \left[C_1 \exp\left(-\frac{\Delta}{k_B T}\right) + C_2 \frac{T}{(T+\theta)}\right]. \quad (5)$$

Taking the θ value from bulk magnetic susceptibility data (Sec. III A or [26]) as 5 K, we can estimate the average spin-gap magnitude of about 73.4 K that is comparable with the value of 65.6 K for the alternating chain model or 76.74 K for the dimer model obtained from the line-shift data at 1.45 T. The sharp upturn of the relaxation rate below 15 K is much stronger than a Curie behavior. It indicates the slowing down of the electron-spin fluctuations and the growth of the correlations of the paramagnetic spins at this temperature region. In the vicinity of the ordering temperature, the correlation length is expected to diverge, and T_1^{-1} in a narrow temperature range (i.e., in the critical regime) can be described by the power law

$$T_1^{-1} \propto \tau^p \quad (6)$$

where $\tau = (T - T_N)/T_N$ and $p = \nu(z - \eta)$ is the critical exponent [56]. The values of ν, z, and η depend upon the dimensionality and the symmetry of the spin lattice and on the type of interactions.

For our data the fit of the relaxation temperature dependence with the formula (6) does not have a unique solution

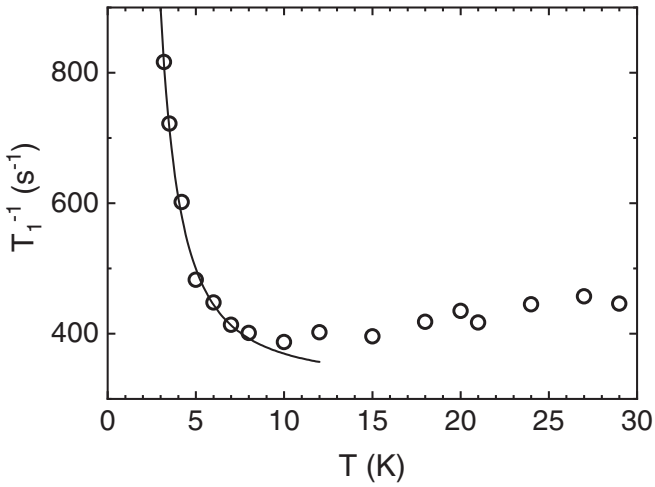

FIG. 10. Low-temperature part of the temperature dependence of the spin-lattice relaxation rate. The solid curve shows the approximations to Eq. (6) with $p = 1.87 \pm 0.193$ and $T_N = 1.03 \pm 0.083$ K (see text for details).

because T_N is unknown and the susceptibility measurements show that T_N, if it exists, is below 2 K. Nevertheless, we tried to apply the model for the critical region formally in order to get an idea of the type of correlations. Using the upper limit for parameter T_N as 1.5 K we fit the curve in the low-temperature region and any reasonable approximations give $p > 1.3$ and $T_N < 1.1$ K (Fig. 10). The best fit of the existing experimental points gives $p = 1.87 \pm 0.193$, which is comparable to $p = 1.93$ for the 2D Ising model ($\nu = 1$, $\eta = 0.25$ [57], $z = 2.18$ [58]) and significantly larger than for three-dimensional (3D) Heisenberg ($\nu = 2/3$ [59,60], $\eta = 0.037$ [60], $z = 3/2$ [61], $p = 0.975$) or 3D Ising ($\nu = 0.6$ [58,62], $\eta = 0.036$, $z = 2.025$ [58], $p = 1.193$) models. Thus, our data evidence in favor of 2D character for critical correlations at low temperatures. It is well known that couplings of the staggered polarization created by spinless impurities in gapped spin chains can induce the growth of the interchain correlations and even the antiferromagnetic long-range order at low temperatures [63]. Such correlated regions are observed in Haldane chains which are very similar to FM-AFM alternating chains and spinless impurities stimulate an antiferromagnetic cluster ordering there due to interaction of these induced moments [17,64]. In $Li_3Cu_2SbO_6$ the alternating FM-AFM chains connect to each other by frustrated AF interaction in the honeycomb magnetic planes. The substitution of the nonmagnetic Li ion for Cu^{2+} in chains cancels frustration of the interchain interaction and leads to growth of the planar correlation. At the same time, the interplanar interaction of randomly arranged defects is apparently not enough for development of strong spin correlations between weakly coupled planes.

IV. THEORY

A. Model and method

To explain the above experimental measurements quantitatively, we construct a spin model taking explicit account of the Cu/Li site inversion in $Li_3Cu_2SbO_6$. If no inversions are considered, the effective model of the magnetic Cu layer is an anisotropic 2D honeycomb Heisenberg model as a bundle of AF-FM alternating Cu chains with assuming rather small interchain couplings. When the inversion is made, each chain in the Cu layer is cut by the Li ions, which behave like nonmagnetic defects, so that the Cu layer is regarded as a set of chain segments. We call this system the *chain-segments spin model*. The Hamiltonian of a chain segment with l sites reads

$$H = \sum_{i=1}^{l-1} J_i \mathbf{S}_i \cdot \mathbf{S}_{i+1}, \tag{7}$$

where $\mathbf{S}_i$ is the spin-$\frac{1}{2}$ operator at site i, and FM ($J_i \equiv J_{FM} < 0$) and AF ($J_i \equiv J_{AF} > 0$) exchange couplings are alternately arranged. As suggested in [26], this system can be essentially mapped onto a $S = 1$ chain segment by regarding two spins coupled by J_{FM} as a spin-1 site. Furthermore, we assume the intercalated Cu^{2+} ions at the original Li sites to have quasifree magnetic moments.

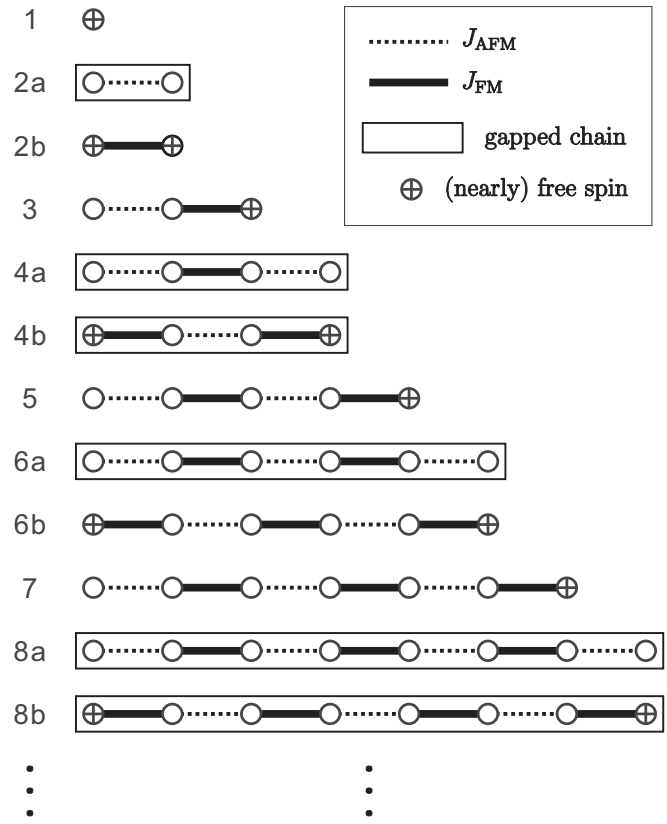

FIG. 11. Lattice structures of FM-AF alternating chain segments. A spin-$\frac{1}{2}$ is localized on each circle. The left characters are indices of the corresponding chain segments. The boxed clusters have a finite gap between the spin-singlet ground state and spin-triplet first excited state.

Examples of the chain segment are shown in Fig. 11. Basically, two spins coupled by J_{AF} form a spin-singlet pair. When l is odd, one of the edge spins is coupled by J_{FM}. Since this edge spin behaves like a free spin, the system is gapless. When l is even, there are two kinds of structures: one is that all spins are involved to form local spin-singlet

pairs by $J_{\rm AF}$ (indexed with 2a, 4a, 6a, 8a, etc.); the other is that both edge spins coupled by $J_{\rm FM}$ are excluded from the formations of local spin-singlet pairs (indexed with 2b, 4b, 6b, 8b, etc.). In the former, the ground state is obviously gapped and the singlet-triplet gap scales to $J_{\rm AF}$. In the latter, more specifically, the system is further classified into two cases $l = 4n$ and $4n + 2$ (n: integer). For $l = 4n$ the entire chain segment forms a spin-singlet state, namely, both edge spins are weakly coupled by AF exchange coupling. Thus, the singlet-triplet gap is tiny but finite and it decreases with increasing l. The singlet-triplet gap for each chain segment is given in Appendix A. For $l = 4n + 2$ both edge spins are completely free and the ground state is gapless.

Using full exact diagonalization technique we calculate the considered physical quantities for each chain segment. Then, the quantities for the magnetic Cu layer can be obtained by summing up contributions from each chain segment. The distribution function of existing probability for a chain segment with l sites is derived by

$$P(l) = \rho \exp\left[-\frac{\rho}{\sqrt{1-\rho}}(l-1)\right], \tag{8}$$

where

$$\rho = \frac{\text{number of Li sites in the Cu layer}}{\text{total number of Li/Cu sites in the Cu layer}}. \tag{9}$$

Note that the length of the chain segment with l sites is $l - 1$. Therefore, a physical quantity for the Cu layer is given as

$$A_{\rm Cu\,layer} = \sum_{l=1}^{l_{\rm max}} A_l \rho \exp\left[-\frac{\rho}{\sqrt{1-\rho}}(l-1)\right], \tag{10}$$

where A_l is the calculated physical quantity for the chain segment with l sites. For even l the quantity is averaged between two possible chains, namely, FM-AF-. . .-AF-FM and AF-FM-. . .-FM-AF. The mean length of chain segments is $\bar{l} = 1/\rho$. Adding to Eq. (10), the magnetic contributions from the intercalated Cu^{2+} ions at Li sites must be taken into account. Each Cu^{2+} ion is assumed to behave like a quasifree magnetic moment and its contribution is equivalent to A_1. Since the ratios of in-layer and out-of-layer Cu^{2+} ions are $1 - \rho$ and ρ, respectively, the physical quantity for the total system is obtained by

$$A_{\rm tot} = \rho A_1 + (1-\rho) A_{\rm Cu\,layer}. \tag{11}$$

B. Fitting of spin susceptibility

First, to estimate the effective parameters we perform a fitting of experimental spin susceptibility at zero field. As shown in Fig. 12 a simple divergent increase of χ with approaching zero temperature is seen in the experimental susceptibility. This behavior is completely different from that of the infinite-length AF-FM alternating chain and the presence of a sufficient amount of free spins may be expected. Let us then determine the effective values of $J_{\rm FM}$, $J_{\rm AF}$, and ρ by the fitting with our chain-segments spin model. The spin susceptibility per spin for a chain segment with l sites is calculated as

$$\chi_l = \frac{1}{lT}\left[\langle S_z^2\rangle - \langle S_z\rangle^2\right], \tag{12}$$

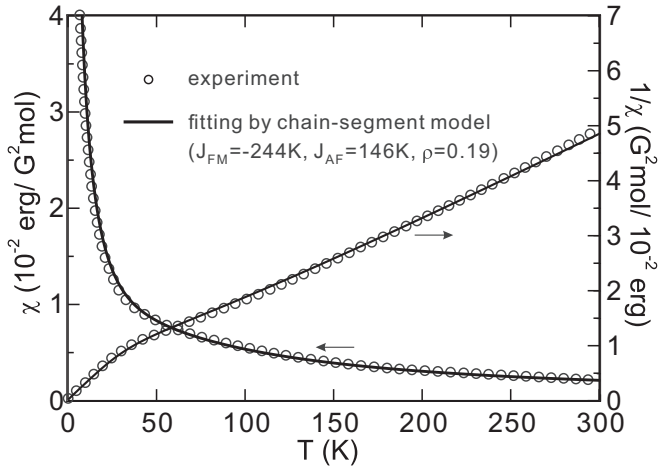

FIG. 12. Fitting of the experimental spin susceptibility by our chain-segments spin model at zero field. A best fitting is achieved setting $J_{\rm FM} = -244$ K, $J_{\rm AF} = 146$ K, and $\rho = 0.19$.

where $\langle \cdots \rangle$ is the canonical average, namely,

$$\langle \hat{\mathcal{O}} \rangle = \frac{1}{Z}\sum_n \hat{\mathcal{O}} \exp\left(-\frac{E_n}{k_B T}\right) \tag{13}$$

with the partition function $Z = \sum_n \exp[-E_n/(k_B T)]$. Since the shape of spin susceptibility depends strongly on $J_{\rm AF}/|J_{\rm FM}|$ and ρ (see Appendix B), a unique fitting is possible. The fitting result is shown in Fig. 12. Setting $J_{\rm FM} = -244$ K, $J_{\rm AF} = 146$ K, and $\rho = 0.19$, a perfect agreement with the experimental susceptibility is obtained. The magnitudes of exchange couplings are somewhat smaller than the previous values $J_{\rm FM} = -285$ K and $J_{\rm AF} = 160$ K estimated with using the infinite-length AF-FM alternating chain. However, a more interesting finding is that 19% of Cu ions are replaced by Li ions. Accordingly, the mean length of the chain segment is only $\bar{l} = 5.25$. Note that in our calculations the chain segments with length up to $l = 15$ are taken into account. This would be indeed a reasonable choice because the existing probability of the chain segment with $l = 15$ is already tiny for $\rho = 0.19$, i.e., $P(15) = 8.0 \times 10^{-3}$. Also, contributions to the spin susceptibility from each of the chain segments are shown in Appendix C.

C. Field- and temperature-dependent magnetization

Next, we examine whether the experimental magnetization can be explained by our chain-segments spin model with the estimated parameters. In Fig. 13(a) the observed and calculated temperature-dependent magnetization curves are compared for several external magnetic fields. The g factor is set to be $g = 2.16$ as an average of $g_\parallel = 2.38$ and $g_\perp = 2.05$ because of the powder sample of $Li_3Cu_2SbO_6$. For all the applied fields the agreement is good over most of the temperature range. This confirms that the dominant exchange couplings of $Li_3Cu_2SbO_6$ are properly contained in our chain-segments spin model. However, as shown in the inset, the agreement becomes worse at very low temperature. The calculated magnetization seems to increase more rapidly as temperature decreases. This may be due to the lack of

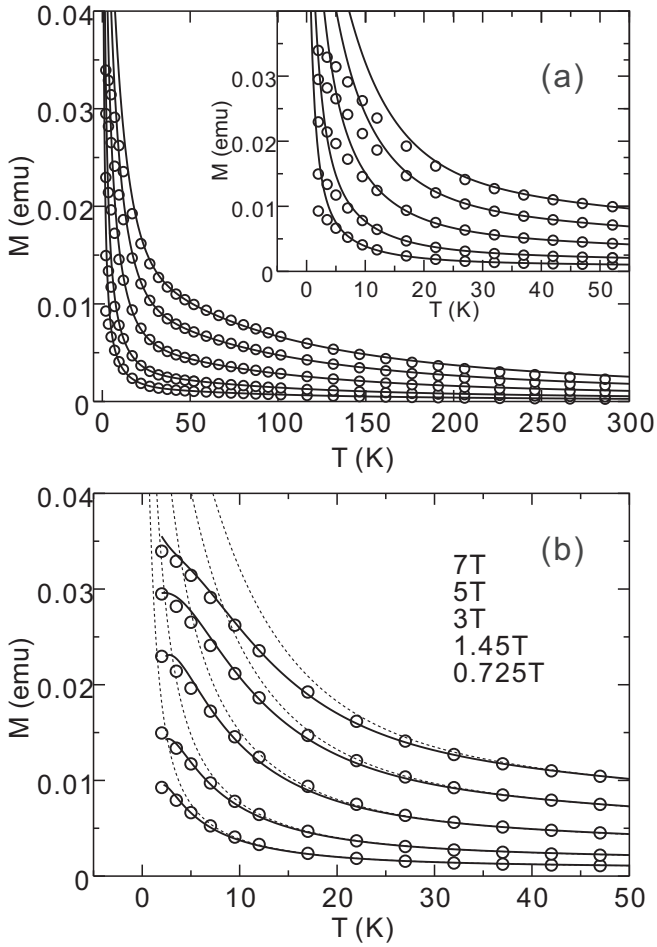

FIG. 13. (a) Fitting of the experimental magnetization curves by our chain-segments spin model with $J_{FM} = -244$ K, $J_{AFM} = 146$ K, and $\rho = 0.19$. The applied external magnetic fields are $B = 0.725$, 1.45, 3, 5, and 7 T from bottom to top. Inset: Enlarged view at low temperature. (b) Similar fitting to (a) with taking into account the effect of interchain coupling. Solid and dotted lines denote the calculated magnetization curves with and without taking into account the effect of interchain coupling (see text).

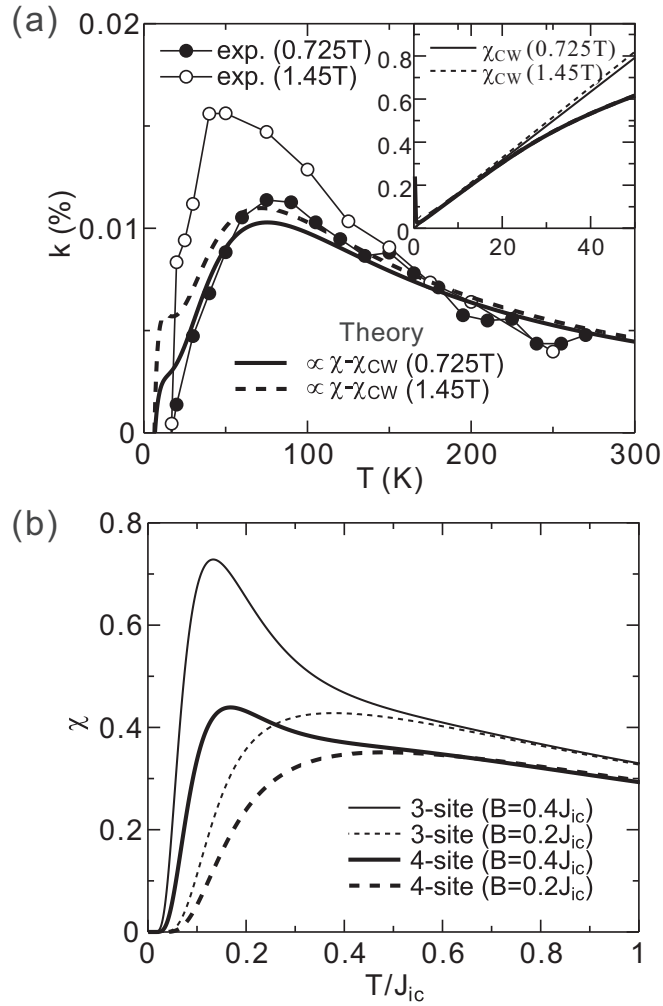

FIG. 14. (a) Comparison between the experimental line shift and the calculated spin susceptibility using our chain-segments spin model with $J_{FM} = -244$ K, $J_{AF} = 146$ K, and $\rho = 0.19$ for $B = 0.725$ and 1.45 T. Inset: Linear fitting of $1/\chi$ at low temperature. (b) Spin susceptibility for three-site and four-site AF open chains at $B/J_{ic} = 0.2$ and 0.4.

small interchain exchange couplings involving the (nearly) free spins in our model. Although it is hard to explicitly introduce the interchain coupling into the spin model, the effect of small interchain coupling is known to be mimicked by a self-consistent staggered magnetic field $(-1)^i h S_i^z$ along the chain, where h is the external-field-dependent local-field strength [65,66]. This corresponds to applying a local mean field $+hS_i^z$ or $-hS_i^z$ on the (nearly) free spins at the edges of chain segments because the spin-singlet pairs in the bulk part of chain segments are not affected by small interchain couplings. Thus, we calculate the interchain-coupling-affected magnetization curve by averaging between the results with applying a local field $+hS_i^z$ and $-hS_i^z$ on the (nearly) free spins. The value of h is tuned to get a reasonable fit of the low-temperature magnetization curve. The amounts of mean field at edges of each chain segment are $h = 2.47$, 3.05, 4.21, 5.95, and 7.54 T for $B = 0.725$, 1.45, 3, 5, and 7 T, respectively. As shown in Fig. 13(b), we see that the qualitative agreement between the observed and calculated magnetization curves is much improved by taking the effect of interchain coupling into account.

D. Field- and temperature-dependent Knight shift

As shown in Fig. 8, the experimental low-field line shift has a peak around $T = 50$ K and the peak height for $B = 1.45$ T is rather higher than that for $B = 0.725$ T. We here attempt a reasonable explanation for these characteristic behaviors with using our chain-segments spin model. The line shift is proportional to the spin susceptibility for the solidly gapped part of the chain segments. Therefore, the Curie-Weiss-like susceptibility at low temperature (χ_{CW}) should be subtracted from the total susceptibility (χ). We estimate the values of χ_{CW} from the slope of $1/\chi$ at low temperature [inset Fig. 14(a)]. Then, the experimental line shifts for $B = 0.725$ and 145 T are compared to the calculated results for $\chi - \chi_{CW}$ in Fig. 14(a). The peak positions roughly coincide. Furthermore, the tendency

toward field dependence seems to be qualitatively consistent but the difference of calculated peak height values for the two fields is rather smaller compared to the experimental line shift. Thus, let us consider the effect of interchain coupling. If the (nearly) free spins are coupled by AF interchain interaction J_{ic}, a number of short AF open chains must be formed over the system. To illustrate contributions to the line shift from such short AF chains, we plot the spin susceptibility for three-site and four-site AF open chains in Fig. 14(b). The field dependence of χ looks similar to that of the experimental line shift. This may indicate that the increase of peak height of the experimental line shift with external field reflects the contribution from short chain segments with coupling J_{ic}, though this is still a qualitative speculation. More quantitative investigations should be done in the future.

E. Specific heat

The specific heat per spin for a chain segment with l sites is calculated as

$$C_l = \frac{1}{lT^2}\left[\langle E_n^2\rangle - \langle E_n\rangle^2\right]. \tag{14}$$

In Fig. 5 the calculated specific heat is compared to the magnetic part of the measured heat capacity C_{mag}. The overall shape including the pronounced peak around $T \sim 45$ K is well reproduced within the framework of our chain-segments spin model. We only see a little discrepancy in the position and height of the small peak at very low temperature. It may be due to the lack of interchain couplings in our spin model, which plays a more important role at lower temperature. Actually, the agreement at low temperature is improved by setting the mean field at segment edges $h = 1.02$ T (Fig. 5).

F. Field-dependent magnetization

Finally, we discuss the magnetization curve as a function of magnetic field. The calculated magnetization curve using the chain-segments spin model is compared to the experimental one in Fig. 3. If we simply calculate M using the chain-segments spin model, the data points marked by filled circles are obtained. The trend is consistent with the experimental curve but the values are a little overestimated. This is again due to the lack of interchain coupling in our spin model. Thus, the agreement could be improved by considering the effect of intersegment coupling. The correction is taken into account as a mean field at the edge of each chain segment. The reestimated data points with the correction are shown with open squares in Fig. 3. We can see a good agreement between theory and experiment. For example, the amounts of the mean field at the edge of each chain segment are $h = 1.60$, 2.18, 3.19, 4.64, and 6.24 T for $B = 0.75$, 1.5, 3.0, 4.5, and 5.0 T, respectively. This means that the AF interchain interaction is about 10 K.

Furthermore, it would be useful to see the full magnetization for the chain-segments spin model. It is shown in Fig. 15. An interesting feature is that a plateaulike feature appears at approximately 1/2 of the full saturation moment. In fact, this tendency has been also found in the experimental magnetization (Fig. 3). At the plateau, the (nearly) free spins at the edges of chain segments are fully polarized along the external field and all of the other remaining spins form spin-singlet pairs. The second onset of the magnetization curve around $B = 50$ T corresponds to the gap of this system. Thus, we can find $\Delta_{AF-FM} = 79.5$ K. This value agrees well with $\Delta_{AF-FM} = 87$ K estimated from the fitting of temperature dependence of the NMR line shift (see Sec. III B).

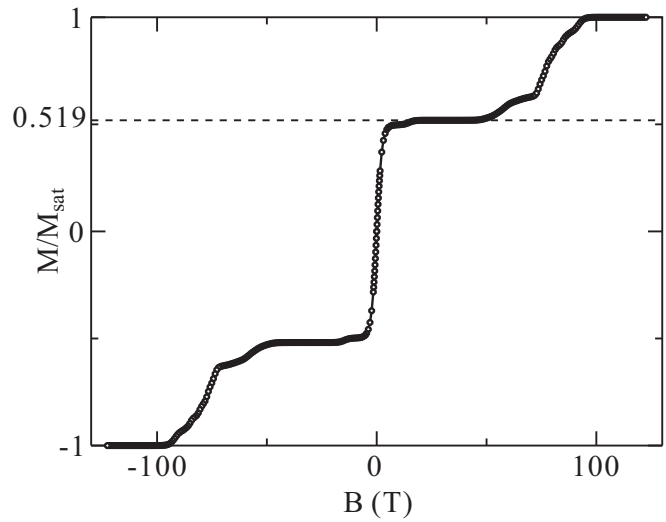

FIG. 15. Field-dependent magnetization curve at $T = 2$ K. Full magnetization curve using the chain-segments spin model with $J_{FM} = -244$ K, $J_{AF} = 146$ K, and $\rho = 0.19$.

Additionally, the magnetization at the plateau ($\equiv M_p/M_{sat}$) is related to the amount of nonmagnetic impurities. Since the magnetization at the plateau corresponds to the polarization of (nearly) free spins at the edges of chain segments, we can simply expect $M_p/M_{sat} \sim 3\rho - 2\rho^2$. In other words, the amount of nonmagnetic impurities can be estimated from the magnetization at the plateau. Actually, as shown in Fig. 15, the M_p/M_{sat} value approximately agrees with $3\rho - 2\rho^2 = 0.498$ obtained by the fitting of magnetic susceptibility.

V. CONCLUSIONS

In summary, we present the results of complex measurements of the ^{7}Li NMR spectra and the spin-lattice relaxation rate in a powder sample of the $Li_3Cu_2SbO_6$ compound with alternating $S = 1/2$ chains containing nonmagnetic defects. Due to the presence of defects in the system under study, several magnetic mechanisms are simultaneously realized, masking the influence of each other and mutually affecting each other. NMR as a local technique makes it possible to unambiguously prove the presence of a clearly pronounced gapped behavior of a spin system with a spin-gap value of about 90 K. The approximation using the AF-FM and noninteracting dimers models gives an acceptable description of the experiments at temperatures above 40 K and makes it possible to estimate the exchange interaction in the system. At the same time, such a simple modeling of the experimental data does not allow for a definite choice: none of the models gives complete agreement over the entire temperature range. The reason for this, apparently, is that the presence of nonmagnetic

inclusions cuts the chains into fragments and generates quasifree spins at their boundaries. Thus the system cannot be described within a framework of the model of infinite chains.

To resolve this problem, we propose a chain-segments spin model consisting of a set of alternating AF-FM chain segments as an effective microscopic model for $Li_3Cu_2SbO_6$. The Hamiltonian of each chain segment is solved by full exact diagonalization technique. From a unique fitting of measured susceptibility, we estimated the interactions as $J_{FM} = -244$ K and $J_{AF} = 146$ K, and found that about 19% of magnetic Cu ions are replaced by nonmagnetic Li ions in $Li_3Cu_2SbO_6$. Using the chain-segments spin model with those parameter values, all of the experimental results like NMR line shift, specific heat, as well as field- and temperature-dependent magnetization can be quantitatively reproduced in a wide temperature range. However, some deviations are seen at very low temperature due to the lack of interchain couplings in our spin model. In order to improve the agreement at very low temperature, we introduced a local field $+hS_i^z$ and $-hS_i^z$ on the (nearly) free spins to mimic the interchain couplings arising from the canceling of its frustration in the vicinity of the defect. The estimated magnitude of interchain couplings is about 10 K. This is confirmed by the observation of the two-dimensional character of correlations in measurements of spin-lattice relaxation at low temperatures.

ACKNOWLEDGMENTS

We thank U. Nitzsche for technical assistance. The work of E.V. and T.S. was supported by Russian Foundation for Basic Research (RFBR) through Grant No. 18-02-00664. S.N. acknowledges support from the German Research Foundation (Deutsche Forschungsgemeinschaft) through SFB 1143 (project No. A05). The work of T.V., E.Z. and A.V. has been supported by the Russian Ministry of Education and Science of Russian Federation, Contract No. 02.A03.21.0011.

E.V. and S.N. made an equal contribution to the paper.

APPENDIX A: SINGLET-TRIPLET GAP OF CHAIN SEGMENTS

Table I shows the singlet-triplet gap, defined by the difference between energies of a ground state with $S = 0$ and an excited state with $S = 1$, for each chain segment with length l. In essence, two neighboring spins coupled by J_{AF} form a spin-singlet pair. When l is odd, $l - 1$ spins are involved to form $(l - 1)/2$ spin-singlet pairs and a spin remains at the segment edge. Since this edge spin behaves like a free spin, the system is gapless. When l is even, the system can be classified broadly into two classes: one is that all spins are involved to form local spin-singlet pairs by J_{AF} (indexed with 2a, 4a, 6a, 8a, etc.); the other is that both edge spins couple by J_{FM} to their neighbors and they are excluded from the formations of local spin-singlet pairs (indexed with 2b, 4b, 6b, 8b, etc.). In the former, the ground state is obviously gapped and the singlet-triplet gap scales to J_{AF} for shorter l and $J_{AF}/2$ for longer l. In the latter, strictly speaking, the system is further classified into two cases $l = 4n$ and $4n + 2$ (n: integer). For $l = 4n$ the entire chain segment forms a spin-singlet state, namely, both edge spins are weakly coupled by AF exchange coupling. Thus, the singlet-triplet gap is tiny but finite. This gap is decreased exponentially with increasing l as expected from the exponential decay of spin-spin correlation with distance in a gapped spin chain. For the remaining case of $l = 4n + 2$, both edge spins are completely free and the ground state is gapless.

TABLE I. Singlet-triplet gap for each chain segment with $J_{FM} = -1$ and $J_{AF} = 0.6$ in the unit of $|J_{FM}|$. Examples of the chain indices are shown in Fig. 11.

Chain index	Singlet-triplet gap
01	0
02a	0.6
02b	0
03	0
04a	0.4539392014169
04b	0.0958874227706
05	0
06a	0.3884147500111
06b	0
07	0
08a	0.3548417721595
08b	0.0224953910776
09	0
10a	0.3351031792316
10b	0
11	0
12a	0.3224735828971
12b	0.0053043323804
13	0
14a	0.3138947996331
14b	0
15	0
16a	0.3078000625086
16b	0.0012304337486

APPENDIX B: ρ AND $J_{AF}/|J_{FM}|$ DEPENDENCE OF SUSCEPTIBILITY

In Fig. 16 the calculated susceptibility of the chain-segments spin model is shown as a function of temperature for $J_{AF}/|J_{FM}| = 0.5$, 1.0, and 2.0. When the density of nonmagnetic impurities ρ is low, the susceptibility consists of two parts; one is a divergent behavior at low temperature and the other is a shoulder peak at intermediate temperature. The divergent behavior is originated from nearly free spins located at the edges of chain segments. On the other hand, the shoulder peak signifies a "bulk" feature of chain segments. Thus, the position of the shoulder peak is shifted to higher temperature with increasing J_{AFM}. This is due to the fact that the undoped AF-FM Heisenberg chain with J_{AF} can be mapped onto a spin-1 spin chain with interaction $J_{AF}/2$. For higher doping ρ, the mean length of chain segments is rapidly reduced, while the number of nearly free spins is rapidly increased. As a result, the shoulder structure as the bulk feature of chain segments is

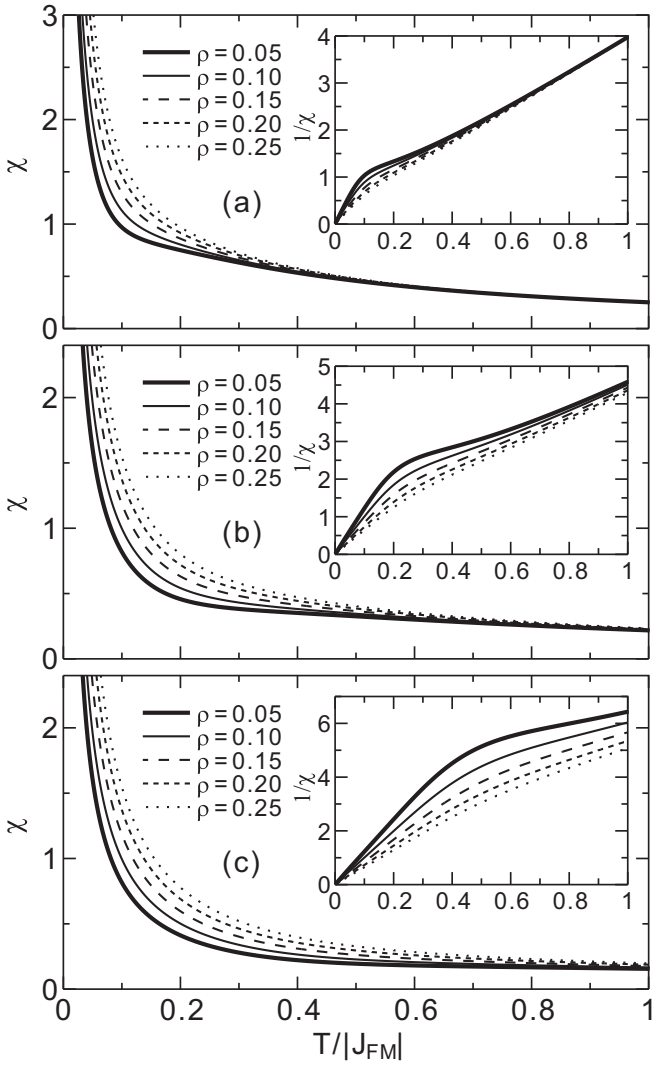

FIG. 16. Calculated susceptibility of the chain-segments spin model as a function of temperature for (a) $J_{AF}/|J_{FM}| = 0.5$, (b) 1.0, and (c) 2.0. Insets: Inverse susceptibility as a function of temperature.

masked by the divergent behavior and is less pronounced even around $\rho = 0.3$.

APPENDIX C: SUSCEPTIBILITY FOR EACH CHAIN SEGMENT

Figure 17 shows the calculated susceptibility for each chain segment indexed in Fig. 11. In the case of odd l [Fig. 17(a)], since the system has a free spin at one edge, a divergent behavior appears at low temperature. Also, there is a broad peak around $T/|J_{FM}| \sim 0.3$ for larger l. This broad peak reveals a reflection of the bulk feature of chain segments, as discussed in the previous section. In the gapped case with even l [Fig. 17(b)], it is clearly seen that the susceptibility goes down to zero at finite temperature and the "critical" temperature is lowered with increasing l. In the gapless case with even l [Fig. 17(c)], the overall tendency seems to be similar to that

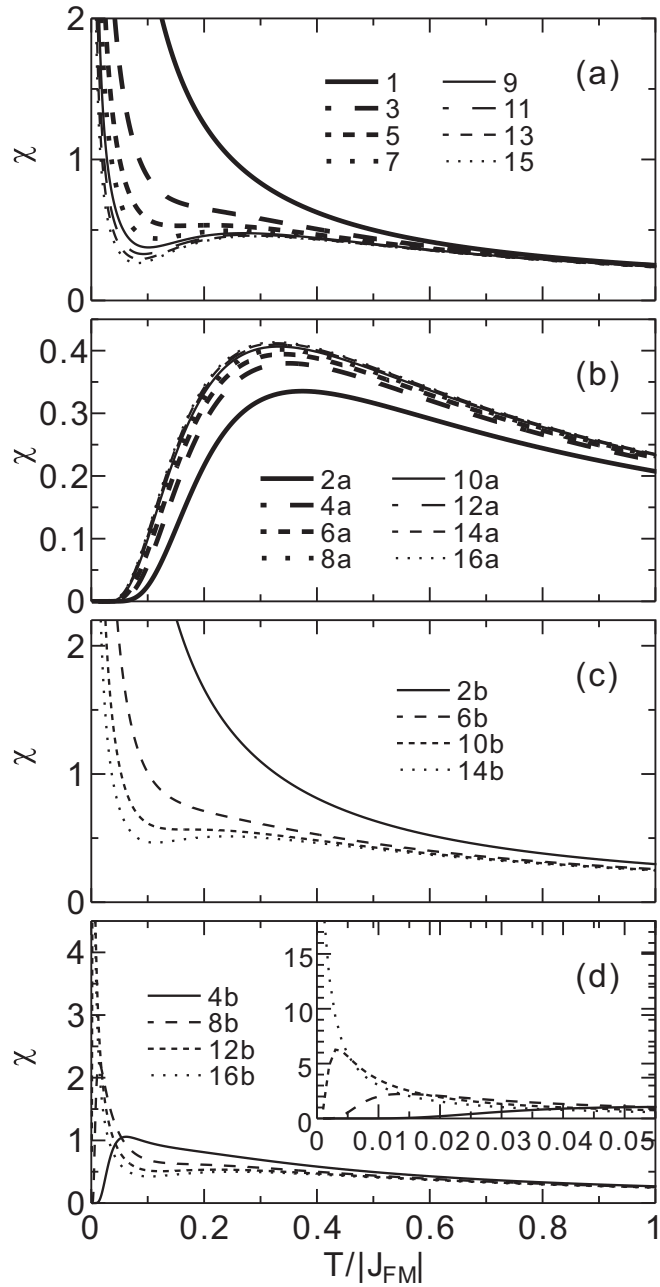

FIG. 17. Calculated susceptibility of the chain-segments spin model with $J_{FM} = -1$ and $J_{AF} = 0.6$ as a function of temperature for (a) odd l and (b–d) even l chain segments. The even l results are further divided into (b) gapped, (c) gapless, and (d) weakly gapped cases. The inset of (d) shows the enlarged view at low temperature.

for odd l chain segments. Interestingly, the divergent behavior at low temperature is even more pronounced than that for the odd l chain segment. Whereas the odd l chain segment has only one free spin at one edge, two spins at both edges are free in the even l gapless chain segment. In the weakly gapped case with even l [Fig. 17(d)], the susceptibility goes down to zero at very low temperature.

[1] J. B. Fouet, P. Sindzingre, and C. Lhuillier, An investigation of the quantum $J_1 - J_2 - J_3$ model on the honeycomb lattice, Eur. Phys. J. B **20**, 241 (2001).

[2] J. Curély, F. Lloret, and M. Julve, Thermodynamics of the two-dimensional Heisenberg classical honeycomb lattice, Phys. Rev. B **58**, 11465 (1998).

[3] R. F. Bishop, P. H. Y. Li, O. Götze, J. Richter, and C. E. Campbell, Frustrated Heisenberg antiferromagnet on the honeycomb lattice: Spin gap and low-energy parameters, Phys. Rev. B **92**, 224434 (2015).

[4] J. Oitmaa and R. R. P. Singh, Phase diagram of the $J_1 - J_2 - J_3$ Heisenberg model on the honeycomb lattice: A series expansion study, Phys. Rev. B **84**, 094424 (2011).

[5] R. Ganesh, J. van den Brink, and S. Nishimoto, Deconfined Criticality in the Frustrated Heisenberg Honeycomb Antiferromagnet, Phys. Rev. Lett. **110**, 127203 (2013).

[6] Z. Zhu, D. A. Huse, and S. R. White, Weak Plaquette Valence Bond Order in the S=1/2 Honeycomb J_1–J_2 Heisenberg Model, Phys. Rev. Lett. **110**, 127205 (2013).

[7] J. Xu, A. Assoud, N. Soheilnia, S. Derakhshan, H. L. Cuthbert, J. E. Greedan, M. H. Whangbo, and H. Kleinke, Synthesis, structure, and magnetic properties of the layered copper(ii) oxide $Na_2Cu_2TeO_6$, Inorg. Chem. **44**, 5042 (2005).

[8] O. Smirnova, V. Nalbandyan, A. Petrenko, and M. Avdeev, Subsolidus phase relations in Na_2O-CuO-Sb_2O_n system and crystal structure of new sodium copper antimonate $Na_3Cu_2SbO_6$, J. Solid State Chem. **178**, 1165 (2005).

[9] Y. Miura, R. Hirai, Y. Kobayashi, and M. Sato, Spin-gap behavior of $Na_3Cu_2SbO_6$ with distorted honeycomb structure, J. Phys. Soc. Jpn. **75**, 084707 (2006).

[10] S. Derakhshan, H. L. Cuthbert, J. E. Greedan, B. Rahaman, and T. Saha-Dasgupta, Electronic structures and low-dimensional magnetic properties of the ordered rocksalt oxides $Na_3Cu_2SbO_6$ and $Na_2Cu_2TeO_6$, Phys. Rev. B **76**, 104403 (2007).

[11] K. Hida, Crossover between the Haldane-gap phase and the dimer phase in the spin-1/2 alternating Heisenberg chain, Phys. Rev. B **45**, 2207 (1992).

[12] S. Watanabe and H. Yokoyama, Transition from Haldane phase to spin liquid and incommensurate correlation in spin-1/2 Heisenberg chains, J. Phys. Soc. Jpn. **68**, 2073 (1999).

[13] Y. Miura, Y. Yasui, T. Moyoshi, M. Sato, and K. Kakurai, Magnetic excitations of spin-gap system $Na_3Cu_2SbO_6$ with distorted honeycomb structure, J. Phys. Soc. Jpn. **77**, 104709 (2008).

[14] M. Schmitt, O. Janson, S. Golbs, M. Schmidt, W. Schnelle, J. Richter, and H. Rosner, Microscopic magnetic modeling for the $s\frac{1}{2}$ alternating-chain compounds $Na_3Cu_2SbO_6$ and $Na_2Cu_2TeO_6$, Phys. Rev. B **89**, 174403 (2014).

[15] T. Goto, N. Fujiwara, T. Kohmoto, and S. Maegawa, Proton spin-lattice relaxation in the quasi-one-dimensional $S = 1$ Heisenberg antiferromagnet $Ni(C_2H_8N_2)_2NO_2(ClO_4)$, J. Phys. Soc. Jpn. **59**, 1135 (1990).

[16] M. Takigawa, T. Asano, Y. Ajiro, M. Mekata, and Y. J. Uemura, Dynamics in the $S = 1$ One-Dimensional Antiferromagnet $AgVP_2S_6$ via ^{31}P and ^{51}V NMR, Phys. Rev. Lett. **76**, 2173 (1996).

[17] F. Lipps, A. H. Arkenbout, A. Polyakov, M. Günther, T. Salikhov, E. Vavilova, H.-H. Klauss, B. Büchner, T. Palstra, and V. Kataev, Magnetic properties of the spin-1 chain compound $NiCl_3C_6H_5CH_2CH_2NH_3$, Low Temp. Phys. **43**, 1298 (2017).

[18] J. A. Quilliam, F. Bert, E. Kermarrec, C. Payen, C. Guillot-Deudon, P. Bonville, C. Baines, H. Luetkens, and P. Mendels, Singlet Ground State of the Quantum Antiferromagnet $Ba_3CuSb_2O_9$, Phys. Rev. Lett. **109**, 117203 (2012).

[19] C. S. Lue, C. N. Kuo, T. H. Su, and G. J. Redhammer, Spin gap behavior in $Cu_2Sc_2Ge_4O_{13}$ studied using ^{45}Sc nuclear magnetic resonance, Phys. Rev. B **75**, 014426 (2007).

[20] J. Kikuchi, K. Motoya, T. Yamauchi, and Y. Ueda, Coexistence of double alternating antiferromagnetic chains in $(VO)_2P_2O_7$: NMR study, Phys. Rev. B **60**, 6731 (1999).

[21] C. S. Lue and B. X. Xie, NMR investigation of $BaCu_2V_2O_8$ in alternating-chain and dimer-chain models, Phys. Rev. B **72**, 052409 (2005).

[22] K. Morimoto, Y. Itoh, K. Yoshimura, M. Kato, and K. Hirota, Hole doping effects on spin-gapped $Na_2Cu_2TeO_6$ via topochemical Na deficiency, J. Phys. Soc. Jpn. **75**, 083709 (2006).

[23] C. Kuo, T. Jian, and C. Lue, Characterization of the spin gap nature in $Na_3Cu_2SbO_6$ using ^{23}Na NMR, J. Alloys Compd. **531**, 1 (2012).

[24] J. M. S. Skakle, M. A. Castellanos R., S. Trujillo Tovar, and A. R. West, Synthesis of $Li_3Cu_2SbO_6$, a new partially ordered rock salt structure, J. Solid State Chem. **131**, 115 (1997).

[25] V. Nalbandyan, M. Avdeev, and M. Evstigneeva, Crystal structure of Li_4ZnTeO_6 and revision of $Li_3Cu_2SbO_6$, J. Solid State Chem. **199**, 62 (2013).

[26] C. Koo, E. A. Zvereva, I. L. Shukaev, M. Richter, M. I. Stratan, A. N. Vasiliev, V. B. Nalbandyan, and R. Klingeler, Static and dynamic magnetic response of fragmented Haldane-like spin chains in layered $Li_3Cu_2SbO_6$, J. Phys. Soc. Jpn. **85**, 084702 (2016).

[27] A. Finkel'stein, V. Kataev, E. Kukovitskii, and G. Teitel'baum, Effects of Zn substitution for Cu atoms in lanthanum-strontium superconductors, Physica C: Superconductivity **168**, 370 (1990).

[28] H. Alloul, J. Bobroff, M. Gabay, and P. J. Hirschfeld, Defects in correlated metals and superconductors, Rev. Mod. Phys. **81**, 45 (2009).

[29] M.-H. Julien, T. Fehér, M. Horvatić, C. Berthier, O. N. Bakharev, P. Ségransan, G. Collin, and J.-F. Marucco, ^{63}Cu NMR Evidence for Enhanced Antiferromagnetic Correlations Around Zn Impurities in $YBa_2Cu_3O_{6.7}$, Phys. Rev. Lett. **84**, 3422 (2000).

[30] I. Affleck, T. Kennedy, E. H. Lieb, and H. Tasaki, Rigorous Results on Valence-Bond Ground States in Antiferromagnets, Phys. Rev. Lett. **59**, 799 (1987).

[31] S. H. Glarum, S. Geschwind, K. M. Lee, M. L. Kaplan, and J. Michel, Observation of Fractional Spin $S = 1/2$ on Open Ends of $S = 1$ Linear Antiferromagnetic Chains: Nonmagnetic Doping, Phys. Rev. Lett. **67**, 1614 (1991).

[32] F. Tedoldi, R. Santachiara, and M. Horvatić, ^{89}Y NMR Imaging of the Staggered Magnetization in the Doped Haldane Chain $Y_2BaNi_{1-x}Mg_xO_5$, Phys. Rev. Lett. **83**, 412 (1999).

[33] M. Kenzelmann, G. Xu, I. A. Zaliznyak, C. Broholm, J. F. DiTusa, G. Aeppli, T. Ito, K. Oka, and H. Takagi, Structure of End States for a Haldane Spin Chain, Phys. Rev. Lett. **90**, 087202 (2003).

[34] A. Smirnov and V. Glazkov, Mesoscopic spin clusters, phase separation, and induced order in spin-gap magnets: A review, J. Exp. Theor. Phys. **105**, 861 (2007).

[35] V. N. Glazkov, A. I. Smirnov, K. Uchinokura, and T. Masuda, Separation of the magnetic phases at the Néel point in the diluted spin-Peierls magnet $CuGeO_3$, Phys. Rev. B **65**, 144427 (2002).

[36] E. F. Shender and S. A. Kivelson, Dilution-Induced Order in Quasi-One-Dimensional Quantum Antiferromagnets, Phys. Rev. Lett. **66**, 2384 (1991).

[37] A. Zorko, D. Arčon, A. Lappas, and Z. Jagličić, Magnetic versus non-magnetic doping effects in the Haldane chain compound $PbNi_2V_2O_8$, New J. Phys. **8**, 60 (2006).

[38] Y. Uchiyama, Y. Sasago, I. Tsukada, K. Uchinokura, A. Zheludev, T. Hayashi, N. Miura, and P. Böni, Spin-Vacancy-Induced Long-Range Order in a New Haldane-Gap Antiferromagnet, Phys. Rev. Lett. **83**, 632 (1999).

[39] M. Takigawa, N. Motoyama, H. Eisaki, and S. Uchida, Field-induced staggered magnetization near impurities in the $S = \frac{1}{2}$ one-dimensional Heisenberg antiferromagnet Sr_2CuO_3, Phys. Rev. B **55**, 14129 (1997).

[40] J. Sirker and N. Laflorencie, NMR response in quasi–one-dimensional spin-$\frac{1}{2}$ antiferromagnets, Europhysics Letters **86**, 57004 (2009).

[41] D. Arcon, A. Zorko, and A. Lappas, ^{51}V NMR study of the doped chain compounds $PbNi_{2-x}Mg_xV_2O_8$, Europhys. Lett. **65**, 109 (2004).

[42] F. Hammerath, S. Nishimoto, H.-J. Grafe, A. U. B. Wolter, V. Kataev, P. Ribeiro, C. Hess, S.-L. Drechsler, and B. Büchner, Spin Gap in the Zigzag Spin-1/2 Chain Cuprate $Sr_{0.9}Ca_{0.1}CuO_2$, Phys. Rev. Lett. **107**, 017203 (2011).

[43] A. Vindigni, A. Rettori, M. Pini, C. Carbone, and P. Gambardella, Finite-sized Heisenberg chains and magnetism of one-dimensional metal systems, Applied Physics A **82**, 385 (2006).

[44] J. Sirker, N. Laflorencie, S. Fujimoto, S. Eggert, and I. Affleck, Chain Breaks and the Susceptibility of $Sr_2Cu_{1-x}Pd_xO_{3+\delta}$ and Other Doped Quasi-One-Dimensional Antiferromagnets, Phys. Rev. Lett. **98**, 137205 (2007).

[45] A. Ghirri, A. Candini, M. Evangelisti, M. Affronte, S. Carretta, P. Santini, G. Amoretti, R. S. G. Davies, G. Timco, and R. E. P. Winpenny, Elementary excitations in antiferromagnetic Heisenberg spin segments, Phys. Rev. B **76**, 214405 (2007).

[46] J. Damerau, F. Göhmann, N. P. Hasenclever, and A. Klümper, Density matrices for finite segments of Heisenberg chains of arbitrary length, J. Phys. A: Math. Theor. **40**, 4439 (2007).

[47] J. Sirker, S. Fujimoto, N. Laflorencie, S. Eggert, and I. Affleck, Thermodynamics of impurities in the anisotropic Heisenberg spin-1/2 chain, J. Stat. Mech.: Theory Exp. **2008**, P02015 (2008).

[48] R. Matysiak, P. Gegenwart, A. Ochiai, M. Antkowiak, G. Kamieniarz, and F. Steglich, Specific heat of segmented Heisenberg quantum spin chains in $(Yb_{1-x}Lu_x)_4As_3$, Phys. Rev. B **88**, 224414 (2013).

[49] N. Stone, Table of nuclear magnetic dipole and electric quadrupole moments, At. Data Nucl. Data Tables **90**, 75 (2005).

[50] A. Tari, *The Specific Heat of Matter at Low Temperatures* (Imperial College, London, 2003), pp. 13545–13553.

[51] E. A. Zvereva, M. I. Stratan, Y. A. Ovchenkov, V. B. Nalbandyan, J.-Y. Lin, E. L. Vavilova, M. F. Iakovleva, M. Abdel-Hafiez, A. V. Silhanek, X.-J. Chen, A. Stroppa, S. Picozzi, H. O. Jeschke, R. Valentí, and A. N. Vasiliev, Zigzag antiferromagnetic quantum ground state in monoclinic honeycomb lattice antimonates $A_3Ni_2SbO_6$ (A=Li, Na), Phys. Rev. B **92**, 144401 (2015).

[52] M. I. Stratan, I. L. Shukaev, T. M. Vasilchikova, A. N. Vasiliev, A. N. Korshunov, A. I. Kurbakov, V. B. Nalbandyan, and E. A. Zvereva, Synthesis, structure and magnetic properties of honeycomb-layered $Li_3Co_2SbO_6$ with new data on its sodium precursor, $Na_3Co_2SbO_6$, New J. Chem. **43**, 13545 (2019).

[53] S. Rommer and S. Eggert, Spin- and charge-density oscillations in spin chains and quantum wires, Phys. Rev. B **62**, 4370 (2000).

[54] J. W. Hall, W. E. Marsh, R. R. Weller, and W. E. Hatfield, Exchange coupling in the alternating-chain compounds catena-di-.μ.-chloro-bis(4-methylpyridine)copper(ii), catena-di-.μ.-bromobis(n-methylimidazole)copper(ii), catena-[hexanedione)bis(thiosemicarbazonato)]copper(ii), and catena-[octanedione bis (thiosemicarbazonato)]copper(ii), Inorg. Chem. **20**, 1033 (1981).

[55] J. J. Borras-Almenar, E. Coronado, J. Curely, R. Georges, and J. C. Gianduzzo, Alternating chains with ferromagnetic and antiferromagnetic interactions. theory and magnetic properties, Inorg. Chem. **33**, 5171 (1994).

[56] F. Borsa, M. Corti, T. Goto, A. Rigamonti, D. C. Johnston, and F. C. Chou, ^{35}Cl NMR study of spin dynamics in $Sr_2CuO_2Cl_2$, Phys. Rev. B **45**, 5756 (1992).

[57] L. Onsager, Crystal statistics. I. A two-dimensional model with an order-disorder transition, Phys. Rev. **65**, 117 (1944).

[58] A. Pelissetto and E. Vicari, Critical phenomena and renormalization-group theory, Phys. Rep. **368**, 549 (2002).

[59] E. Riedel and F. Wegner, Dynamic Scaling Theory for Anisotropic Magnetic Systems, Phys. Rev. Lett. **24**, 730 (1970).

[60] M. Campostrini, M. Hasenbusch, A. Pelissetto, P. Rossi, and E. Vicari, Critical exponents and equation of state of the three-dimensional Heisenberg universality class, Phys. Rev. B **65**, 144520 (2002).

[61] P. C. Hohenberg and B. I. Halperin, Theory of dynamic critical phenomena, Rev. Mod. Phys. **49**, 435 (1977).

[62] H. Benner and J. Boucher, in *Magnetic Properties of Layered Transition Metal Compounds*, edited by L. D. Jongh (Springer, New York, 1990), pp. 323–378.

[63] J. Bobroff, N. Laflorencie, L. K. Alexander, A. V. Mahajan, B. Koteswararao, and P. Mendels, Impurity-Induced Magnetic Order in Low-Dimensional Spin-Gapped Materials, Phys. Rev. Lett. **103**, 047201 (2009).

[64] A. I. Smirnov, V. N. Glazkov, H.-A. Krug von Nidda, A. Loidl, L. N. Demianets, and A. Y. Shapiro, Paramagnetic and antiferromagnetic resonances in the diamagnetically diluted Haldane magnet $PbNi_2V_2O_8$, Phys. Rev. B **65**, 174422 (2002).

[65] H. J. Schulz, Dynamics of Coupled Quantum Spin Chains, Phys. Rev. Lett. **77**, 2790 (1996).

[66] M. Bocquet, F. H. L. Essler, A. M. Tsvelik, and A. O. Gogolin, Finite-temperature dynamical magnetic susceptibility of quasi-one-dimensional frustrated spin-$\frac{1}{2}$ Heisenberg antiferromagnets, Phys. Rev. B **64**, 094425 (2001).